

Singularity-free and cosmologically viable Born-Infeld gravity with scalar matter

David Benisty^{1, 2, 3, *} Gonzalo J. Olmo^{4, 5, †} and Diego Rubiera-Garcia^{6, ‡}

¹*DAMTP, Centre for Mathematical Sciences, University of Cambridge, Wilberforce Road, Cambridge CB3 0WA, United Kingdom*

²*Frankfurt Institute for Advanced Studies (FIAS), Ruth-Moufang-Strasse 1, 60438 Frankfurt am Main, Germany*

³*Physics Department, Ben-Gurion University of the Negev, Beer-Sheva 84105, Israel*

⁴*Departamento de Física Teórica and IFIC, Centro Mixto Universidad de Valencia - CSIC. Universidad de Valencia, Burjassot-46100, Valencia, Spain*

⁵*Departamento de Física, Universidade Federal da Paraíba, 58051-900 João Pessoa, Paraíba, Brazil*

⁶*Departamento de Física Teórica and IPARCOS, Universidad Complutense de Madrid, E-28040 Madrid, Spain*

(Dated: March 1, 2025)

The early Cosmology driven by a single scalar field, both massless and massive, in the context of Eddington-inspired Born-Infeld gravity, is explored. We show the existence of nonsingular solutions of bouncing and loitering type (depending on the sign of the gravitational theory's parameter) replacing the Big Bang singularity, and discuss their properties. In addition, in the massive case we find some new features of the cosmological evolution depending on the value of the mass parameter, including asymmetries in the expansion/contraction phases, or a continuous transition between a contracting phase to an expanding one via an intermediate loitering phase. We also provide a combined analysis of cosmic chronometers, standard candles, BAO, and CMB data to constrain the model, finding that for roughly $|\epsilon| \lesssim 10^{-4}$ the model is compatible with the latest observations while successfully removing the Big Bang singularity.

I. INTRODUCTION

The standard concordance cosmological Λ CDM model, framed within Einstein's General Theory of Relativity (GR), including an early phase of inflationary expansion, a cold dark matter component, and a tiny cosmological constant driving the accelerated late-time expansion of the Universe, has successfully met all observations [1, 2]. Within this model, scalar fields have found new and imaginative applications. For instance, inflationary models in the early Universe involve from one to many scalar fields [3–12]. In the slow-roll approximation the exact form of the scalar field potential is unknown since many different potentials have been studied and confronted to observations. On the other hand, a way to parameterize dark energy is by using a scalar field, the so-called quintessence model (for canonical scalar fields [13, 14]) or its generalizations to K-essence models (when a non-canonical scalar Lagrangian is considered [15–18]), in such a way that the cosmological constant gets replaced by a dark energy fluid with a nearly constant density today [19–23]. Dark matter can be also parameterized in terms of weakly-interacting massive particles, which can be scalar particles still undiscovered at colliders and other dark matter detection experiments. Models for dark matter can also be based on other kinds of scalar fields, for instance, via fuzzy dark matter [24], or by using a Lagrange multiplier that changes the behaviour of the kinetic term [25–28]. Scalar field models may also be the result of com-

plex effective interactions of other fundamental fields in equilibrium, such as in Bose-Einstein condensates, thus allowing for an even broader range of phenomenological justifications.

Despite its observational success, from a fundamental point of view the Λ CDM model still contains a visible singularity at the Universe's past. This is an unavoidable consequence of the singularity theorems (see e.g. [29] for a pedagogical discussion). It is widely assumed that at the strong curvatures and fields of the very early Universe, quantum gravity effects should come into play in order to regularize this singularity. Since a quantum theory of gravity is not available yet, an effective way to capture such hypothetical effects is via modified theories of gravity [30–33]. The plausibility of such models to supersede GR and represent observationally viable alternatives to the Λ CDM model has been widely discussed in the literature [34].

Among the large pool of theories which have been investigated in the literature, for the sake of this paper we bring here the proposal originally introduced by Banados and Ferreira [35] and dubbed as Eddington-inspired Born-Infeld (EiBI) gravity. In order to avoid troubles with ghost-like instabilities, this theory is typically formulated in metric-affine spaces, where metric and affine connection are a priori independent entities. EiBI theory has found many different applications in astrophysics and cosmology, see e.g. [36–45]. In particular, the existence of bouncing solutions replacing the Big Bang singularity within EiBI gravity was first hinted in [46], in particular, when scalar fields are considered as the matter source. The main aim of this work is to construct explicit such solutions corresponding to a single massless (quintessential) scalar field, and to further extend (numerically) this

* benidav@post.bgu.ac.il

† gonzalo.olmo@uv.es

‡ drubiera@ucm.es

analysis to the massive case. We shall show the existence of two kinds of singularity-free solutions depending on the sign of the EiBI gravity parameter. The first one corresponds to bouncing solutions, where the universe contracts down to a minimum size before entering into an expansion phase, while the second are loitering solutions, which interpolate between an asymptotically Minkowski past and the current cosmological evolution. For these nonsingular solutions we carry out a combined analysis of cosmic chronometers, standard candles, BAO, and CMB data in order to constrain the EiBI parameter.

This paper is organized as follows: in Sec. II we introduce EiBI gravity, discuss its properties, and construct its cosmological equations when coupled to a scalar field. In Sec. III we consider massless scalar fields and discuss its corresponding bouncing and loitering solutions, extending these results in Sec. IV to the massive case. Sec. V sees the theory fit with the latest observations (on Λ CDM background), and we conclude in Sec. VI with a summary and some perspectives.

II. EDDINGTON-INSPIRED BORN-INFELD GRAVITY

A. Action and basic field equations

The action of EiBI gravity can be conveniently written as

$$\mathcal{S}_{EiBI} = \frac{1}{\epsilon\kappa^2} \int d^4x [\sqrt{-q} - \lambda\sqrt{-g}] + \mathcal{S}_m(g_{\mu\nu}, \psi_m), \quad (1)$$

where $\kappa^2 \equiv 8\pi G/c^4$ is Newton's constant, ϵ is a parameter with dimensions of length squared, g is the determinant of the space-time metric $g_{\mu\nu}$ and q the determinant of an auxiliary metric defined as:

$$q_{\mu\nu} \equiv g_{\mu\nu} + \epsilon R_{(\mu\nu)}(\Gamma), \quad (2)$$

where the (symmetric part of the) Ricci tensor $R_{\mu\nu}(\Gamma) \equiv R^\rho_{\mu\rho\nu}(\Gamma)$ is a function solely of the (torsionless) affine connection $\Gamma \equiv \Gamma^\lambda_{\mu\nu}$, assumed to be *a priori* independent of the space-time metric $g_{\mu\nu}$ (metric-affine or Palatini formalism). This symmetrizing requirement ensures that the theory is invariant under projective transformations, which avoids the presence of ghost-like instabilities [47]. As for the matter sector, $\mathcal{S}_m = \int d^4x \sqrt{-g} \mathcal{L}_m(g_{\mu\nu}, \psi_m)$, it is assumed to be minimally coupled to the space-time metric $g_{\mu\nu}$, with ψ_m denoting collectively the matter fields. It is worth pointing out that EiBI gravity recovers the GR dynamics and its solutions in the $|R_{\mu\nu}| \ll \epsilon^{-1}$ limit, inheriting an effective cosmological constant $\Lambda_{eff} = \frac{\lambda-1}{\epsilon\kappa^2}$.

EiBI gravity is nowadays a very well known theory in the community thanks to its many applications (for a detailed account of its properties we refer the reader to the review [48]). It is actually a member of the so-called Ricci-based family of gravitational theories [49], all of

which admit an Einstein-like representation of their field equations given by

$$G^\mu_{\nu}(q) = \frac{\kappa^2}{|\Omega|^{1/2}} \left[T^\mu_{\nu} - \delta^\mu_\nu \left(\mathcal{L}_G + \frac{T}{2} \right) \right], \quad (3)$$

where \mathcal{L}_G is the gravitational Lagrangian, $T_{\mu\nu} = \frac{2}{\sqrt{-g}} \frac{\delta S_m}{\delta g^{\mu\nu}}$ is the stress-energy tensor of the matter fields, T its trace, and $G^\mu_{\nu}(q)$ is the Einstein tensor of the auxiliary metric $q_{\mu\nu}$, such that Γ is Levi-Civita of it, that is

$$\nabla_\alpha (\sqrt{-q} q^{\mu\nu}) = 0. \quad (4)$$

This $q_{\mu\nu}$ metric is related to the space-time one $g_{\mu\nu}$ via the relation

$$q_{\mu\nu} = g_{\mu\alpha} \Omega^\alpha_{\nu}, \quad (5)$$

where the *deformation* matrix $\hat{\Omega}$ (with $|\Omega|$ denoting its determinant) depends on-shell on the matter fields (and possibly the space-time metric $g_{\mu\nu}$ as well). For EiBI gravity this matrix is implicitly determined via the equation

$$|\Omega|^{1/2} (\Omega^{-1})^\mu_{\nu} = \lambda \delta^\mu_\nu - \epsilon \kappa^2 T^\mu_{\nu}, \quad (6)$$

while the EiBI Lagrangian in (1) can also be expressed in terms of this matrix as

$$\mathcal{L}_G = \frac{|\Omega|^{1/2} - \lambda}{\epsilon \kappa^2}. \quad (7)$$

Let us point out that all terms on the right-hand side of the equations (3) are functions of the matter fields and the metric $g_{\mu\nu}$, thus representing a system of second-order field equations with new couplings engendered by the matter fields. In vacuum, $T^\mu_{\nu} = 0$, one recovers the GR solutions, which ensures the propagation of the two polarizations of the gravitational field travelling at the speed of light [50].

B. EiBI cosmology with scalar fields

As the matter sector of our model let us consider a single (real) scalar field described by the action

$$\mathcal{S}_m = -\frac{1}{2} \int d^4x \sqrt{-g} \mathcal{L}_m = -\frac{1}{2} \int d^4x \sqrt{-g} (X + 2V(\phi)), \quad (8)$$

with kinetic term $X \equiv g^{\mu\nu} \partial_\mu \phi \partial_\nu \phi$ and scalar potential $V(\phi)$. The variation of this action with respect to the scalar field leads to the field equations

$$\frac{1}{\sqrt{-g}} \partial_\mu (\sqrt{-g} g^{\mu\nu} \partial_\nu \phi) = V_\phi, \quad (9)$$

(where $V_\phi \equiv dV/d\phi$) and to the associated stress-energy tensor

$$T^\mu_{\nu} = g^{\mu\alpha} \partial_\alpha \phi \partial_\nu \phi - \frac{\mathcal{L}_m}{2} \delta^\mu_\nu. \quad (10)$$

We consider next a spatially flat Friedman-Lemaitre-Robertson-Walker (FLRW) space-time, with line element:

$$ds_g^2 \equiv g_{\mu\nu} dx^\mu dx^\nu = -dt^2 + a^2(t) d\vec{x}^2, \quad (11)$$

where $a(t)$ is the expansion factor and $d\vec{x}^2 = \delta_{ij} dx^i dx^j$, with $i, j = 1 \dots 3$ for the spatial part. As from now on we shall assume $\phi = \phi(t)$, the stress-energy tensor (10) reads:

$$T^\mu_{\nu} = \begin{pmatrix} -\frac{1}{2}\dot{\phi}^2 - V & 0 \\ 0 & (\frac{1}{2}\dot{\phi}^2 - V)I_{3 \times 3} \end{pmatrix}. \quad (12)$$

where a dot denotes a derivative with respect to t , as usual.

From Eq.(6) we can conclude that the deformation matrix needs to have a similar algebraic (diagonal) structure as that of the stress-energy tensor of the scalar field, namely

$$\Omega^\mu_{\nu} = \begin{pmatrix} \Omega_+ & 0 \\ 0 & \Omega_- I_{3 \times 3} \end{pmatrix}, \quad (13)$$

where the identity matrix $I_{3 \times 3}$ represents the spatial sector. Now, plugging this ansatz and Eq.(12) into Eq.(6) gives the components of this matrix as:

$$\Omega_-^2 = \left(\lambda + \epsilon\kappa^2 V - \frac{\epsilon\kappa^2 \dot{\phi}^2}{2} \right) \left(\lambda + \epsilon\kappa^2 V + \frac{\epsilon\kappa^2 \dot{\phi}^2}{2} \right) = \left(\tilde{\lambda}^2 - \Phi^2 \right) \quad (14)$$

$$\Omega_+^2 = \frac{\left(\lambda + \epsilon\kappa^2 V - \frac{\epsilon\kappa^2 \dot{\phi}^2}{2} \right)^3}{\left(\lambda + \epsilon\kappa^2 V + \frac{\epsilon\kappa^2 \dot{\phi}^2}{2} \right)} = \frac{\left(\tilde{\lambda} - \Phi \right)^3}{\left(\tilde{\lambda} + \Phi \right)}, \quad (15)$$

where we have used the shorthand notations

$$\tilde{\lambda} \equiv \lambda + \epsilon\kappa^2 V \quad (16)$$

$$\Phi \equiv \frac{\epsilon\kappa^2 \dot{\phi}^2}{2}. \quad (17)$$

Therefore, we are ready to cast the field equations (3) for this problem as

$$\epsilon R^\mu_{\nu}(q) = \begin{pmatrix} 1 - \frac{(\tilde{\lambda} + \Phi)}{|\Omega|^{1/2}} & 0 \\ 0 & \left(1 - \frac{(\tilde{\lambda} - \Phi)}{|\Omega|^{1/2}} \right) \delta^i_j \end{pmatrix}, \quad (18)$$

where the determinant of the deformation matrix reads $|\Omega|^{1/2} = \Omega_+^{1/2} \Omega_-^{3/2}$. Now, to compute the left-hand side of the field equations (18) one can write another line element for the auxiliary metric also of the FLRW form, that is

$$ds_q^2 \equiv q_{\mu\nu} dx^\mu dx^\nu = -dT^2 + \tilde{a}^2(T) d\vec{x}^2 = -\Omega_+(t) dt^2 + a^2(t) \Omega_-(t) d\vec{x}^2, \quad (19)$$

where in the second line we have used the fundamental relation (5) together with the ansatz (13). These gravitational field equations must be supplemented with the

scalar field equations (9) which, in the FLRW background (11), read

$$\ddot{\phi} + 3\frac{\dot{a}}{a}\dot{\phi} + V_\phi = 0. \quad (20)$$

Now, using the fact that in the $q_{\mu\nu}$ geometry (19) we have the well known formulas

$$R^t_t \equiv \frac{3}{\tilde{a}} \frac{d^2 \tilde{a}}{dT^2} \quad (21)$$

$$R^i_i \equiv \frac{1}{\tilde{a}} \frac{d^2 \tilde{a}}{dT^2} + \frac{2}{\tilde{a}^2} \left(\frac{d\tilde{a}}{dT} \right)^2, \quad (22)$$

with the relations

$$\frac{d\tilde{a}}{dT} = \frac{1}{\Omega_+^{1/2}} \frac{d}{dt} \left(a\Omega_-^{1/2} \right) \quad (23)$$

$$\frac{d^2 \tilde{a}}{dT^2} = \frac{1}{\Omega_+^{1/2}} \frac{d}{dt} \left[\frac{1}{\Omega_+^{1/2}} \frac{d}{dt} \left(a\Omega_-^{1/2} \right) \right], \quad (24)$$

it follows that the combination

$$3R^i_i - R^t_t \equiv \frac{6}{\Omega_- \Omega_+} \left(\frac{d\tilde{a}}{dT} \right)^2, \quad (25)$$

can be written as

$$3R^i_i - R^t_t \equiv \frac{6}{\Omega_- \Omega_+} \left[\frac{1}{a} \frac{d}{dt} \left(a\Omega_-^{1/2} \right) \right]^2, \quad (26)$$

and a little algebra leads to

$$\frac{1}{a} \frac{d}{dt} \left(a\Omega_-^{1/2} \right) = \frac{1}{\Omega_-^{3/2}} \left[\frac{\dot{a}}{a} \left(\tilde{\lambda}^2 + 2\Phi^2 \right) + \left(\tilde{\lambda} + \Phi \right) \frac{\Phi V_\phi}{\dot{\phi}} \right],$$

which allows us to find an expression for $H \equiv \dot{a}/a$ as

$$H = \frac{1}{\left(\tilde{\lambda}^2 + 2\Phi^2 \right)} \left[-\left(\tilde{\lambda} + \Phi \right) \frac{\Phi V_\phi}{\dot{\phi}} \pm \Omega_-^2 \sqrt{\frac{\Omega_+}{3\epsilon} \left(|\Omega|^{1/2} - \left(\tilde{\lambda} - 2\Phi \right) \right)} \right]. \quad (27)$$

The square of this quantity is the generalized FLRW equation for EiBI gravity coupled to a scalar field with a potential $V(\phi)$. The \pm signs in front of the square root yield expanding (+) or contracting (-) universes and must be chosen on physical grounds. In the limit $\epsilon \rightarrow 0$ the above expression yields

$$H = \pm \sqrt{\frac{\kappa^2 (\dot{\phi}^2 + 2V)}{6}}, \quad (28)$$

which recovers the FLRW dynamics of GR coupled to a scalar field.

Note that, from Eq.(12), for a scalar field the energy density ρ_ϕ and pressure P_ϕ are related to the field variables by

$$\rho_\phi \equiv \frac{\dot{\phi}^2}{2} + V \quad (29)$$

$$P_\phi \equiv \frac{\dot{\phi}^2}{2} - V, \quad (30)$$

which allows to write the quantities inside the functions Ω_{\pm} of Eqs. (14) and (15) in terms of ρ_ϕ and P_ϕ as

$$\tilde{\lambda} + \Phi = \lambda + \epsilon \kappa^2 \rho_\phi \quad (31)$$

$$\tilde{\lambda} - \Phi = \lambda - \epsilon \kappa^2 P_\phi. \quad (32)$$

III. MASSLESS SCALAR FIELDS

To explicitly solve the gravitational and scalar field equations (18) and (9) we need to specify a form of the scalar potential $V(\phi)$. For the sake of simplicity, and to make contact with similar settings in black hole scenarios [51], let us consider first the case of a free scalar field, $V = 0$, for which the scalar field equation (11) has a first integral

$$\dot{\phi} = \frac{\dot{\phi}_0}{a^3(t)}, \quad (33)$$

with $\dot{\phi}_0$ an integration constant. Since in this case $P_\phi = \rho_\phi = \dot{\phi}^2/2$, the components of the deformation matrix (13) assume the relatively simple form

$$\Omega_- = \left(\lambda^2 - \frac{\rho_\phi^2}{\rho_\epsilon^2} \right)^{\frac{1}{2}}; \quad \Omega_+ = \frac{\left(\lambda - s \frac{\rho_\phi}{\rho_\epsilon} \right)^{3/2}}{\left(\lambda + s \frac{\rho_\phi}{\rho_\epsilon} \right)^{1/2}}, \quad (34)$$

where we have defined the critical density $\rho_\epsilon = 1/(\kappa^2|\epsilon|)$ and $s = \pm 1$ denotes the sign of ϵ . The corresponding Hubble function takes the form

$$H^2 = \frac{\left(\lambda^2 - \frac{\rho_\phi^2}{\rho_\epsilon^2} \right)^{3/2} \left(\lambda - s \frac{\rho_\phi}{\rho_\epsilon} \right)^2}{3s\epsilon \left(\lambda^2 + 2\frac{\rho_\phi^2}{\rho_\epsilon^2} \right)^2} \quad (35)$$

$$\times \left(\left(\lambda - s \frac{\rho_\phi}{\rho_\epsilon} \right) \sqrt{\lambda^2 - \frac{\rho_\phi^2}{\rho_\epsilon^2}} - \lambda + 2s \frac{\rho_\phi}{\rho_\epsilon} \right).$$

As mentioned before, at low densities as compared to the scale ρ_ϵ , this equation recovers the GR expression, which can be solved leading to the approximate solution $a(t) = H_0 t^{1/3}$. The Hubble factor here can be conveniently set to $H_0^2 = 3\kappa^2 \dot{\phi}_0^2/2$ to adjust the integration constant $\dot{\phi}_0$ in order to reproduce the standard cosmological evolution of GR coupled to a massless scalar field. At higher densities, however, the dynamics strongly departs from that of GR and it is evident that when the energy density of the scalar field approaches its maximum value, $\rho_\phi = \lambda \rho_\epsilon$, the Hubble function vanishes. This corresponds to a minimum value of the expansion factor for both branches of solutions $s = \pm 1$, but there are two different mechanisms by which the initial Big Bang singularity is avoided, which we discuss next. For simplicity, from now on we focus on asymptotically flat configurations, $\lambda = 1$.

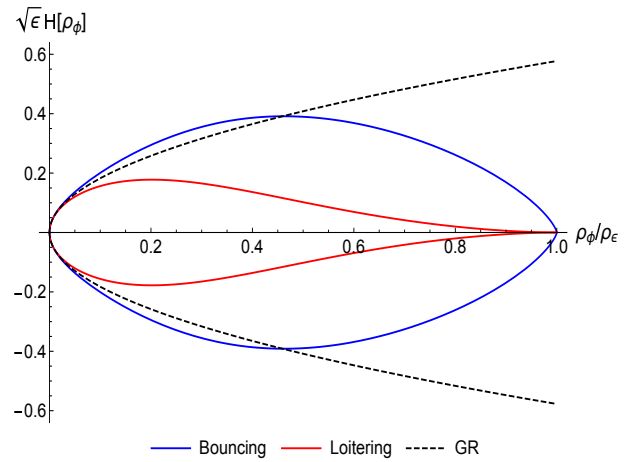


Figure 1. Representation of the Hubble function $\sqrt{|\epsilon|} H(\rho_\phi)$ vs. the energy density for EiBI gravity (solid) and GR (dashed) with massless scalar field as a function of the ratio ρ_ϕ/ρ_ϵ . Note how the trajectories of the EiBI theory are bounded, while that of GR (dashed black) is open. Bouncing solutions (blue) reach the maximum density forming a $\pi/2$ angle with the horizontal axis, while the loitering branch (red) reaches it tangentially.

For the $s = -1$ branch, at the critical density $\rho_\phi = \rho_\epsilon$, the Hubble factor in Eq.(35) and its derivative behave as

$$H(\rho_\phi) \approx \pm \frac{2^{7/4}}{3|\epsilon|^{1/2}} \left(1 - \frac{\rho_\phi}{\rho_\epsilon} \right)^{3/4} \quad (36)$$

$$\frac{dH}{d\rho_\phi} \approx \mp \frac{1}{2^{1/4} |\epsilon|^{1/2} \rho_\epsilon \left(1 - \frac{\rho_\phi}{\rho_\epsilon} \right)^{1/4}}. \quad (37)$$

This indicates that at the maximum achievable density, $\rho_\phi = \rho_\epsilon$, the Hubble factor vanishes while its derivative goes to infinity. This implies that the universe contracts to a minimum (maximum) value of the expansion factor (energy density), before re-expanding. This is the typical behaviour expected in standard bouncing solutions with a transition from a contracting phase to an expanding one, where the universe could even undergo a sequence of cyclic cosmologies with both phases. In Fig. 1 we plot the form of $H(\rho)$ (blue curves) to show that while at late-times (i.e. low densities, $\rho_\phi \ll \rho_\epsilon$) these solutions converge to those of GR (in agreement to Eq.(28)), at high densities ($\rho_\phi/\rho_\epsilon \rightarrow 1$) they depart from the standard Big Bang singularity of GR.

For the $s = +1$ branch we find that the evolution of the Hubble factor as we approach the maximum density $\rho_\phi = \rho_\epsilon$ is given instead by

$$H(\rho_\phi) \approx \pm \frac{2^{3/4} \sqrt{\frac{1}{\epsilon}} \left(1 - \frac{\rho_\phi}{\rho_\epsilon} \right)^{7/4}}{3\sqrt{3}} \quad (38)$$

$$\frac{dH}{d\rho_\phi} \approx \mp \frac{7 \sqrt{\frac{1}{\epsilon}} \left(1 - \frac{\rho_\phi}{\rho_\epsilon} \right)^{3/4}}{6 \sqrt[4]{2} \sqrt{3} \rho_\epsilon}, \quad (39)$$

which means that the Hubble factor vanishes there as well, but instead of being divergent its derivative takes a finite value (which is actually zero). This implies that the expansion factor reaches a fixed value $a(t) = a_m$, corresponding to an asymptotically Minkowski past, and starts expanding as we move forward in time after some reference time $t = t_p$. In Fig. 1 we depict this behaviour (red curves) of these so-called loitering solutions, where the qualitative differences with the bouncing solutions are manifest. Again, at late times (low densities) the standard GR evolution is recovered. Therefore we see that a free massless scalar field coupled to EiBI gravity is able to yield nonsingular evolutions in both $s = \pm 1$ branches according to these two mechanisms, something not possible within GR.

IV. MASSIVE SCALAR FIELD

Let us now consider a massive scalar field with a potential of the form

$$V(\phi) = \frac{1}{2}\mu^2\phi^2, \quad (40)$$

where μ is a constant. In this case, the Hubble function (27) develops an explicit dependence on both ρ_ϕ and P_ϕ [to lighten the notation from now on we shall drop the label ϕ in these quantities] via Eqs.(31) and (32). Since the resulting expression does not provide any useful insight, we will not write it explicitly here. Instead, for the sake of comparison with the massless case of the previous section, we find it more illustrative to provide a parametric representation of $H(t)$ versus $\rho(t)$. These functions are obtained by numerically integrating the second-order equation for \ddot{a} that follows from (22) together with its corresponding right-hand side. The result of the integration is used to construct the quantity \dot{a}/a , which is then compared with the formula (27) to check the consistency of the numerical integration. Again we split our discussion of the corresponding results into the $s = \pm 1$ cases.

In Figs. 2 and 3, we show the function $H(\rho(t))$ for solutions corresponding to several values of the reduced mass $\sigma \equiv \mu^2/\rho_\epsilon$ in the case $s = -1$. The corresponding expansion factors $a(t)$ appear in Fig. 4, while in Fig. 5 we show the function $\dot{a}(t)$ of those same examples and in Fig. 6 their Hubble functions. As one can see from all these plots, the case $s = -1$ still represents bouncing solutions for all the mass range explored, which goes from $\sigma \approx 10^{-8}$ up to $\sigma \approx 0.4$, with little variations with respect to the massless scenario for masses as high as $\sigma \approx 10^{-3}$ (see Fig. 2). For higher masses, the egg-shaped Hubble function develops a fish-like structure, with asymmetric fins. This asymmetry is also manifest in the contracting branch of the expansion factor (see Fig. 4), which becomes increasingly asymmetric as the mass parameter grows from zero. A similar behaviour can be observed in the density profiles of the scalar field depicted in Fig. 7.

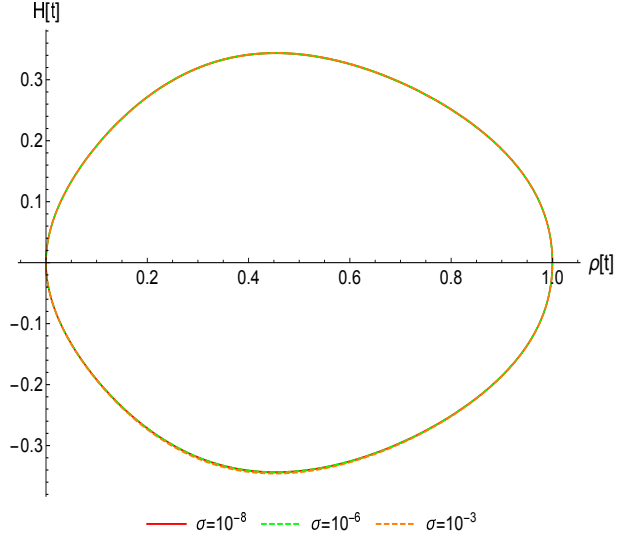


Figure 2. Parametric plot of $\sqrt{|\epsilon|}H(t)$ as a function of $\rho(t)/\rho_\epsilon$ for small masses when $s = -1$ (bouncing solutions). The (reduced) mass parameter is taken such that $\sigma \equiv \mu^2/\rho_\epsilon$.

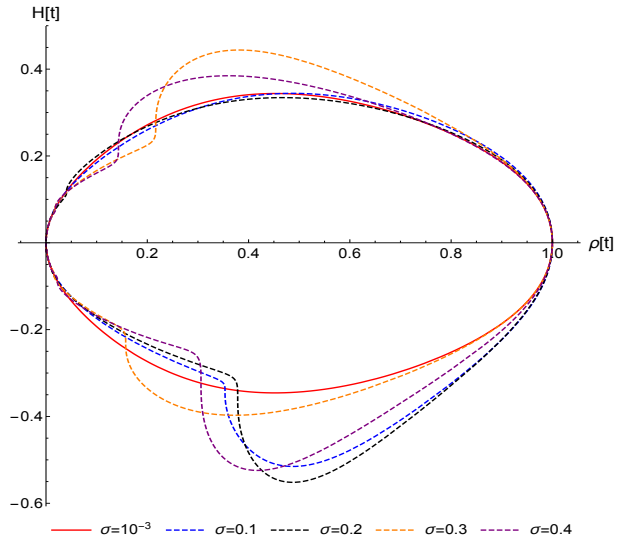


Figure 3. Parametric plot of $H(t)$ as a function of $\rho(t)$ for larger values of the reduced mass $\sigma \equiv \mu^2/\rho_\epsilon$ when $s = -1$.

Focusing now on the case with $s = +1$, which represents loitering solutions in the massless case, Fig. 8 shows that the function $H(\rho(t))$ is now qualitatively different (compare to Fig. 1). Indeed, when $\sigma = 0$, $H(t)$ never crosses the horizontal axis as one approaches the maximum allowed energy density. However, for $\sigma \neq 0$ one either has an expanding branch which starts from an almost constant $a(t) = a_m$ initial phase or a contracting phase that ends up in an almost constant final $a(t) = a_m$. Now we observe that *all* solutions develop a bounce at some high density, effectively crossing the axis and establishing a continuous transition from a contracting phase to an expanding one. The loitering phase, with an almost constant $a(t)$, may last for a long period after

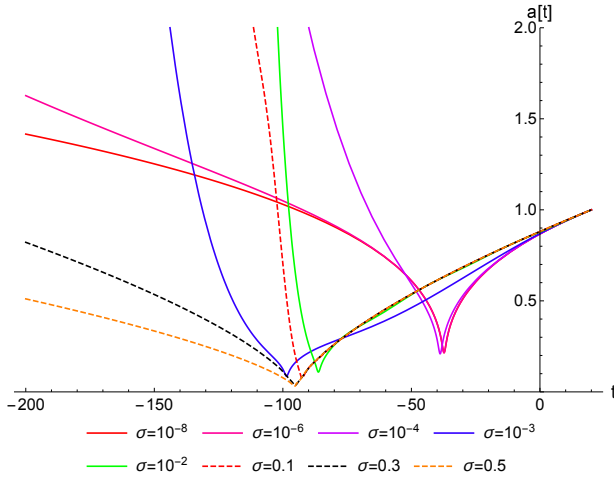


Figure 4. Expansion factor $a(t)$ representing bouncing solutions for various values of the reduced mass parameter $\sigma \equiv \mu^2/\rho_\epsilon$ when $s = -1$.

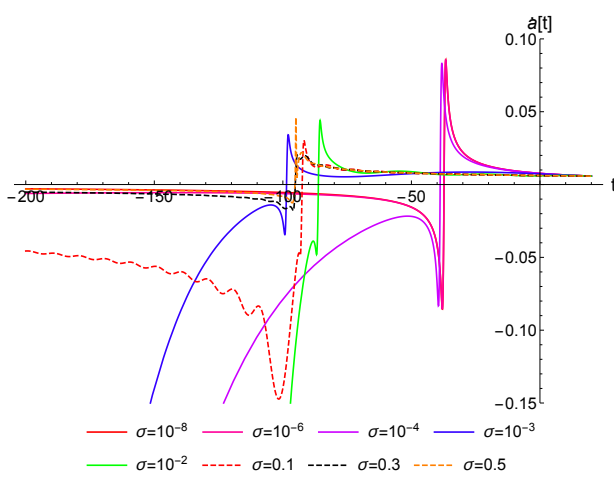


Figure 5. Time derivative of the expansion factor representing bouncing solutions for various values of the reduced mass parameter $\sigma \equiv \mu^2/\rho_\epsilon$. The colors of the curves are the same as in Fig. 4. Note that the blue and magenta curves will bounce at some point and begin a growing oscillatory trajectory similar to that of the red dashed curve, being this a generic behavior of all these solutions.

an initial contraction but it will always end up in an expanding branch. This is illustrated in Fig. 9, where the blue dashed curve represents a phase with $a(t)$ almost constant for a long time (very low mass). The orange curve has essentially the same future behaviour as the blue curve but its loitering phase (almost constant expansion factor) does not last so much, exhibiting a previously contracting phase that arises abruptly. Similar behaviours arise for larger masses, and one verifies that the instabilities in the expansion factor always lead to a bounce, never finding fully collapsed solutions. This is a remarkable property of the EiBI model, since it always avoids the development of singular solutions.

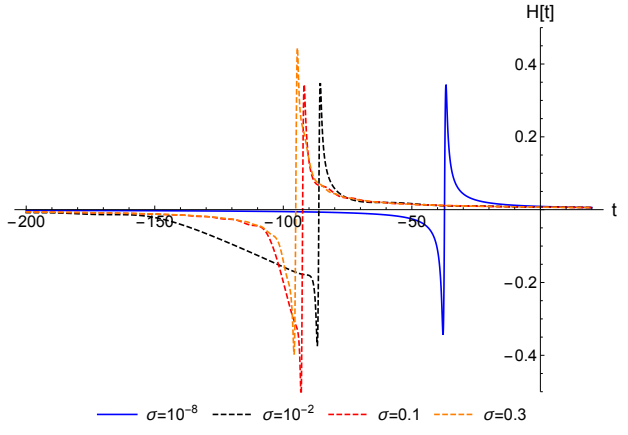


Figure 6. Hubble function $H \equiv \dot{a}/a$ for various values of the reduced mass parameter $\sigma \equiv \mu^2/\rho_\epsilon$ of the $s = -1$ case.

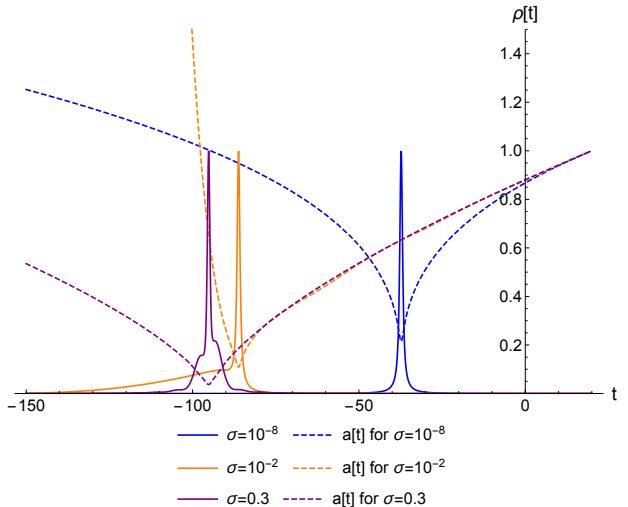


Figure 7. Energy density (solid curves) as a function of time superimposed with its corresponding expansion factor $a(t)$ (dashed curves) for some bouncing solutions of the $s = -1$ case.

For completeness, the behaviour of $\dot{a}(t)$ and $H(t)$ for this case $s = +1$ are shown in Figs. 10 and 11. The corresponding energy density profiles appear in Figs. 12 and 13. It is amusing to see how for low mass configurations (orange solid curve, for instance) the energy density at early times is very low (large universe with very diluted energy) until it rapidly increases to reach a maximum, where it stays for some time at an almost constant value (loitering phase) with a slight decay (decompression) as we move forward in time. Then the density suddenly drops again giving rise to an expanding phase. For larger values of the scalar field mass, this process can be significantly deformed but the qualitative features remain.

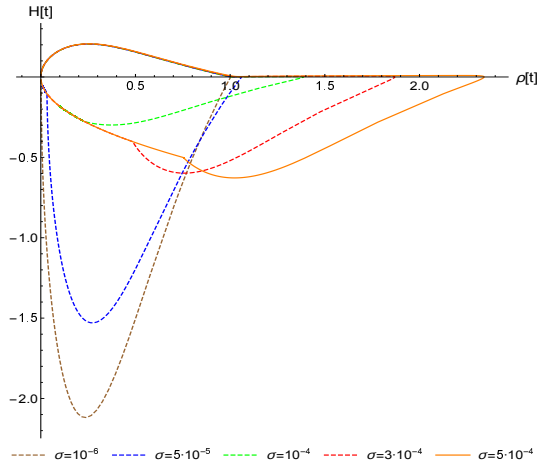


Figure 8. Parametric plot of $H(t)$ as a function of $\rho(t)$ for small values of the reduced mass σ of the $s = +1$ case.

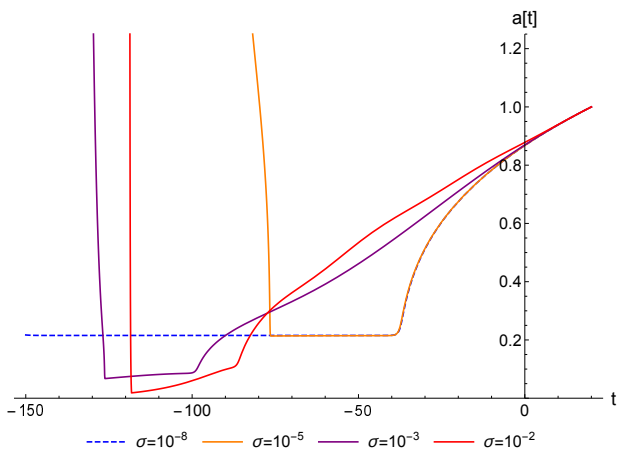


Figure 9. Expansion factor representing new bouncing solutions for various values of the reduced mass parameter σ when $s = +1$.

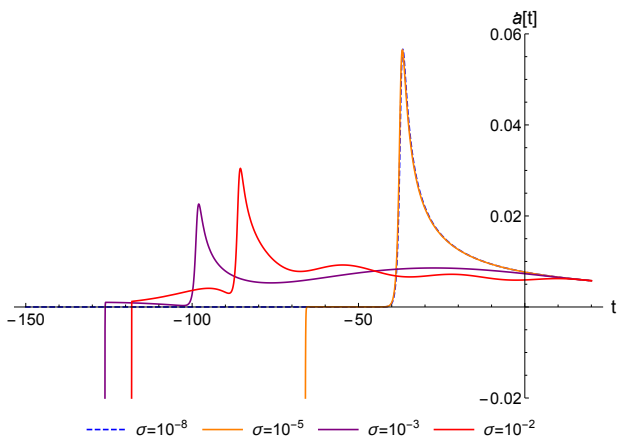


Figure 10. Time derivative of the expansion factor representing bouncing solutions for the reduced mass parameter σ when $s = +1$.

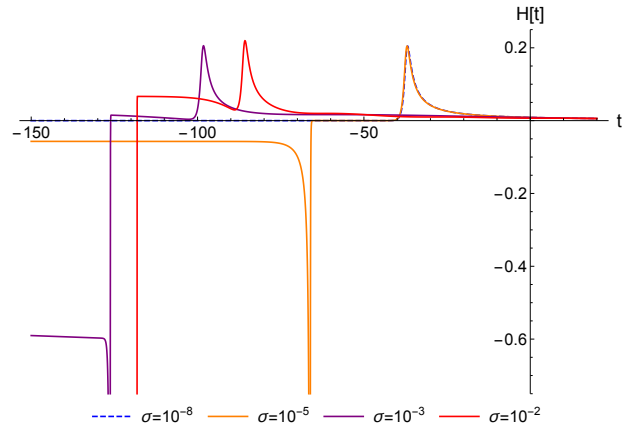


Figure 11. Hubble function \dot{a}/a for various values of the reduced mass parameter σ when $s = +1$.

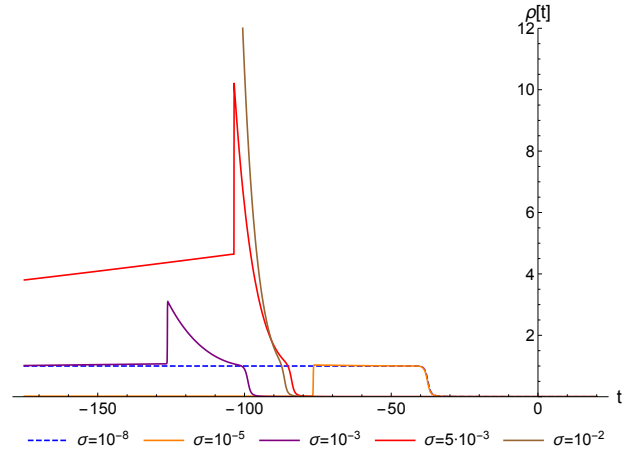


Figure 12. Energy density (solid curves) as a function of time superimposed with its corresponding expansion factor $a(t)$ (dashed curves).

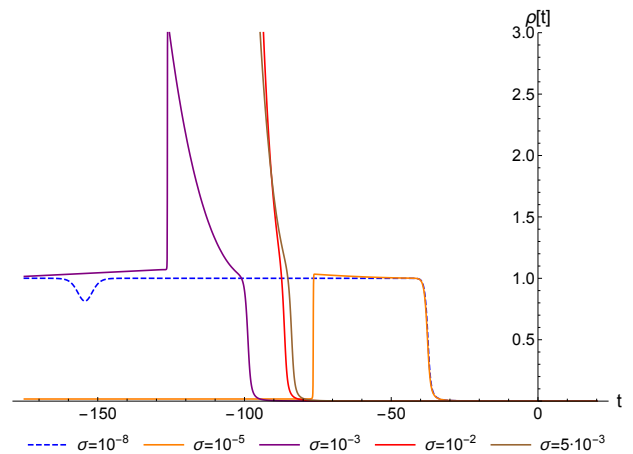


Figure 13. Zoom in of the energy density (solid curves) as a function of time superimposed with its corresponding expansion factor $a(t)$ (dashed curves).

V. OBSERVATIONAL CONSTRAINTS

In this section we shall put to observational test the EiBI cosmologies considered in the previous sections by using the latest observational data to constraint the EiBI parameter ϵ preventing the singularity in the early Universe. The matter fields considered are the dark energy Ω_Λ , dark matter Ω_m , and radiation Ω_r components. The corresponding energy density reads

$$\frac{\rho}{\rho_c} = \frac{\Omega_m}{a^3} + \frac{\Omega_r}{a^3} + \Omega_\Lambda . \quad (41)$$

Inserting this equation in the expression of the Hubble factor (27), and assuming a small EiBI parameter, $|R_{\mu\nu}| \ll \epsilon^{-1}$, yields the extended Friedman equation:

$$\begin{aligned} \frac{H^2}{H_0^2} &= \frac{\Omega_m}{a^3} + \frac{\Omega_r}{a^3} + \Omega_\Lambda \\ &+ \epsilon \left(\frac{9\Omega_m^2}{8a^6} + \frac{\Omega_m\Omega_r}{a^7} - \frac{2\Omega_\Lambda\Omega_r}{a^4} \right) + \mathcal{O}(\epsilon^2) , \end{aligned} \quad (42)$$

where the EiBI corrections to GR solutions are apparent.

We now proceed to describe the observational data sets along with the relevant statistics in constraining the model.

- Cosmic Chronometers (CC): This data set exploits the evolution of differential ages of passive galaxies at different redshifts to directly constrain the Hubble parameter [53]. We use uncorrelated 30 CC measurements of $H(z)$ discussed in [54–57].
- As Standard Candles (SC) we use measurements of the Pantheon type Ia supernova [58], that were collected in [59], as well as quasars [60] and gamma ray bursts [61]. The model parameters are fitted by comparing the observed μ_i^{obs} value to the theoretical μ_i^{th} value of the distance moduli, which are the logarithms:

$$\mu = m - M = 5 \log_{10}(D_L) + \mu_0 , \quad (43)$$

where m and M are the apparent and absolute magnitudes and $\mu_0 = 5 \log(H_0^{-1}/Mpc) + 25$ is the nuisance parameter that has been marginalized. The luminosity distance is defined by

$$D_L(z) = \frac{c}{H_0} (1+z) \int_0^z \frac{dz'}{E(z')} , \quad (44)$$

(here $\Omega_k = 0$, i.e., a flat space-time and $E(z)$ is the dimensionless Hubble parameter). For the SNIa data the covariance matrix is not diagonal and the distance modulus is given as $\mu_i = \mu_{B,i} - \mathcal{M}$, where $\mu_{B,i}$ is the apparent magnitude at maximum in the rest frame for redshift z_i and \mathcal{M} is treated as a universal free parameter, quantifying various observational uncertainties [58]. It is apparent that

the \mathcal{M} and H parameters are intrinsically degenerate in the context of the Pantheon data set, so we cannot extract any information regarding H_0 from SNIa data alone.

- We use uncorrelated data points from different Baryon Acoustic Oscillations (BAO). BAO are a direct consequence of the strong coupling between photons and baryons in the pre-recombination epoch. After the decoupling of photons, the over densities in the baryon fluid evolved and attracted more matter, leaving an imprint in the two-point correlation function of matter fluctuations with a characteristic scale of around $r_d \approx 147$ Mpc that can be used as a standard ruler and to constrain cosmological models. Studies of the BAO feature in the transverse direction provide a measurement of $D_H(z)/r_d = c/H(z)r_d$, with the comoving angular diameter distance [62, 63]:

$$D_M = \int_0^z \frac{c dz'}{H(z')} . \quad (45)$$

The angular diameter distance $D_A = D_M/(1+z)$ and the quantity $D_V(z)/r_d$ with

$$D_V(z) \equiv [zD_H(z)D_M^2(z)]^{1/3} \quad (46)$$

are a combination of the BAO peak coordinates above. The surveys provide the values of the measurements at some effective redshift. We employ the BAO data points collected in [64] from [65–76], in the redshift range $0.106 < z < 2.34$. The BAO scale is set by the sound horizon at the drag epoch $z_d \approx 1060$ when photons and baryons decouple. In our analysis we used r_d as independent parameter.

- Finally we take the Cosmic Microwave Background (CMB) distant prior measurements [77]. The distance priors provide effective information of the CMB power spectrum in two aspects: the acoustic scale l_A characterizes the CMB temperature power spectrum in the transverse direction, leading to the variation of the peak spacing, and the “shift parameter” R influences the CMB temperature spectrum along the line-of-sight direction, affecting the heights of the peaks, which are defined as follows:

$$l_A = (1+z_d) \frac{\pi D_A(z_d)}{r_d} , \quad (47)$$

$$R(z_d) = \frac{\sqrt{\Omega_m} H_0}{c} (1+z_d) D_A(z_d) , \quad (48)$$

with its corresponding covariance matrix (see table I in [77]).

In order to perform a joint statistical analysis of these four cosmological probes we need to use the total likelihood function. Regarding the problem of likelihood

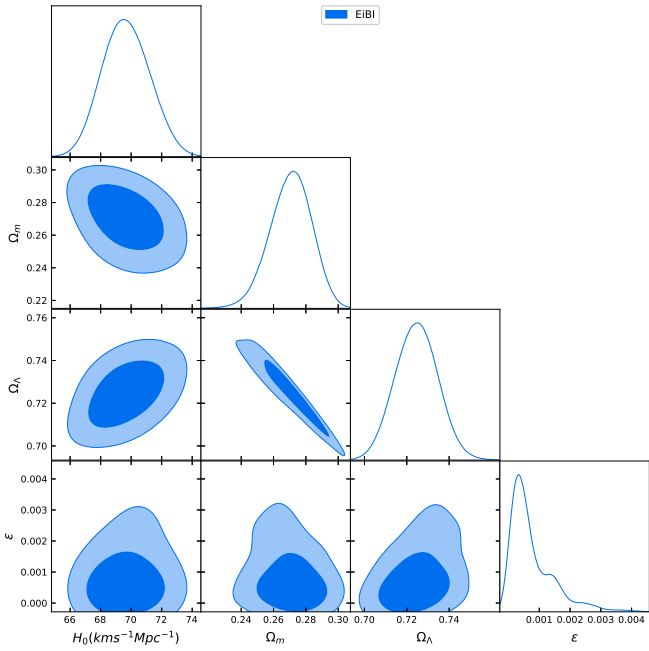


Figure 14. The posterior distribution for the Hubble parameter H_0 vs. the EiBI parameter ϵ .

maximization, we use an affine-invariant Markov Chain Monte Carlo sampler [78], as it is implemented within the open-source packaged *Polychord* [79] with the *GetDist* package [80] to present the results. The prior we choose is with a uniform distribution, where $\Omega_m \in [0.; 1.]$, $\Omega_\Lambda \in [0.; 1 - \Omega_m]$, $H_0 \in [50; 100]$ Km/sec/Mpc, and $r_d \in [130; 160]$ Mpc. For the EiBI parameter ϵ we set the range $\epsilon \in [0.; 0.01]$.

The posterior distribution of H_0 vs. the EiBI parameter ϵ is presented in Fig. 14. The Hubble parameter is $H_0 = 69.25 \pm 1.315$ km/sec/Mpc which is in between the Planck estimation of the Hubble function [2] and the latest SH0ES measurement [81]. The dark matter component is $\Omega_m = 0.2749 \pm 0.0106$ and the dark energy component is being $\Omega_\Lambda = 0.7213 \pm 0.0851$. The fit for the EiBI parameter gives $\epsilon = (6.155 \pm 7.263) \cdot 10^{-4}$. We point out that the value of $\epsilon = 0$ (which corresponds to GR) is very close to the mean value. Therefore, for $|\epsilon| \lesssim 10^{-4}$ the theory is able to fit to the data while being able to successfully remove the Big Bang singularity.

VI. CONCLUSION AND DISCUSSION

In this paper we have analyzed homogeneous and isotropic cosmological solutions in the context of Eddington-inspired Born-Infeld gravity coupled to a single scalar field. In the massless case we discussed the existence and properties of such solutions by direct resolution of the modified gravitational field equations, which depend on the sign of the EiBI parameter. For the bouncing solutions ($s = -1$) one finds that at the maximum

achievable density of the scalar field the expansion factor gets to a minimum non-vanishing value (vanishing Hubble factor) undergoing a transition from a contracting phase to an expanding one (or vice versa). In the loitering solutions ($s = +1$) the cosmological evolution starts from an asymptotically Minkowski past with a minimum constant value of the expansion factor, such that at a given time a canonical cosmological expansion phase is triggered. These results are consistent with the expectancy raised in the seminal paper [35] and the numerical evidence found in more recent works [82] when considering perfect fluids as the matter source.

Though the massless case was known to have only two types of solutions, namely, bouncing and loitering, some kind of instability was expected for the loitering case beyond the massless scenario. Until now it was not known if they would lead to singular solutions or if they would remain nonsingular. Our analysis puts forward that the model is absolutely robust against singularities and that the loitering case gives rise to a new type of solutions in which an unstable Minkowskian phase (almost constant expansion factor) is possible in between a contraction phase and an expansion phase. The duration of this Minkowskian period (see Fig. 9) depends on model parameters and the initial conditions. No singular solutions are found in our analysis, neither in the massless nor in the massive case. All the nonsingular solutions recover the late-time GR cosmological evolution.

Getting into the details, for the $s = -1$ branch we found that for low masses the solutions closely resemble the behaviour of those of the massless case. However, for masses above a certain threshold the parametric representation of the Hubble function versus the energy density develops a kind of fish-like asymmetric fins at certain time in the cosmological evolution, a feature not present in the massless case (compare Fig. 1 with Figs. 2 and 3). The $s = +1$ branch also exhibits unusual features, showing that during the loitering (almost Minkowskian) phase the energy density can grow significantly while the Hubble function remains close to zero and positive (see Fig. 8). This represents a kind of intermediate state in a continuous transition from a contracting phase to a final expansion one. This behaviour is triggered by the energy density stored in the massive scalar field, whose drop marks the end of the loitering phase and the beginning of the expansion phase (see Figs. 12 and 13).

To conclude, the results obtained in this paper further support the effectiveness of EiBI gravity to remove singularities in cosmological and astrophysical scenarios when coupled to different matter sources. In the present scenario with scalar fields this can be done while being consistent with the latest cosmological observations provided that the EiBI parameter is kept roughly within $|\epsilon| \lesssim 10^{-4}$. One important aspect of the obtained solutions not tackled here is whether they are stable under tensorial perturbations or not. We point out that in the present case the equation of state is of the form $\omega = \omega(t)$ since the energy density and the pressure of the scalar

field (in the massive case) are not trivially related. In turn this should have an impact on the behaviour of the quantities prone to the development of instabilities in the tensorial perturbations equation, such as the sound speed [82, 83]. This analysis would further support the feasibility of this theory and their associated solutions to replace the Big Bang singularity by observationally viable nonsingular cosmologies.

ACKNOWLEDGEMENTS

DB gratefully acknowledges the support from the Blavatnik and the Rothschild fellowship. GJO is no longer funded by the Ramon y Cajal contract RYC-2013-13019 (Spain) because he already became permanent. DRG is funded by the *Atracción de Talento*

Investigador programme of the Comunidad de Madrid (Spain) No. 2018-T1/TIC-10431, and acknowledges further support from the Ministerio de Ciencia, Innovación y Universidades (Spain) project No. PID2019-108485GB-I00/AEI/10.13039/501100011033, and the FCT projects No. PTDC/FIS-PAR/31938/2017 and PTDC/FIS-OUT/29048/2017. This work is supported by the Spanish project FIS2017-84440-C2-1-P (MINECO/FEDER, EU), the project PROMETEO/2020/079 (Generalitat Valenciana), the project i-COOPB20462 (CSIC) and the Edital 006/2018 PRONEX (FAPESQ-PB/CNPQ, Brazil, Grant 0015/2019). This article is based upon work from COST Action CA18108, supported by COST (European Cooperation in Science and Technology). DB thanks the Department of Theoretical Physics of the Complutense University of Madrid for their hospitality during the elaboration of this work.

[1] L. Amendola, *et al.* [Euclid Theory Working Group], *Living Rev. Rel.* **16** (2013) 6.

[2] N. Aghanim, *et al.* [Planck Collaboration], [arXiv:1807.06209](https://arxiv.org/abs/1807.06209) [astro-ph.CO].

[3] A. A. Starobinsky, *JETP Lett.* **30** (1979) 682 [*Pisma Zh. Eksp. Teor. Fiz.* **30** (1979) 719].

[4] A. A. Starobinsky, *Phys. Lett.* **91B** (1980) 99 [*Adv. Ser. Astrophys. Cosmol.* **3** (1987) 130].

[5] A. D. Linde, *Phys. Lett.* **108B** (1982) 389 [*Adv. Ser. Astrophys. Cosmol.* **3** (1987) 149].

[6] A. H. Guth, *Phys. Rev. D* **23** (1981) 347 [*Adv. Ser. Astrophys. Cosmol.* **3** (1987) 139].

[7] A. Albrecht and P. J. Steinhardt, *Phys. Rev. Lett.* **48** (1982) 1220 [*Adv. Ser. Astrophys. Cosmol.* **3** (1987) 158].

[8] V. F. Mukhanov and G. V. Chibisov, *JETP Lett.* **33** (1981) 532 [*Pisma Zh. Eksp. Teor. Fiz.* **33** (1981) 549].

[9] A. H. Guth and S. Y. Pi, *Phys. Rev. Lett.* **49** (1982) 1110.

[10] J. D. Barrow, *Nucl. Phys. B* **296** (1988) 697.

[11] J. D. Barrow and S. Cotsakis, *Phys. Lett. B* **214** (1988) 515.

[12] E. Elizalde, S. Nojiri, S. D. Odintsov, D. Saez-Gomez and V. Faraoni, *Phys. Rev. D* **77** (2008) 106005.

[13] B. Ratra and P. J. E. Peebles, *Phys. Rev. D* **37** (1988) 3406.

[14] R. R. Caldwell, R. Dave and P. J. Steinhardt, *Phys. Rev. Lett.* **80** (1998) 1582.

[15] J. Kehayias and R. J. Scherrer, *Phys. Rev. D* **100** (2019) 023525.

[16] V. K. Oikonomou and N. Chatzarakis, *Nucl. Phys. B* **956** (2020) 115023.

[17] A. Chakraborty, A. Ghosh and N. Banerjee, *Phys. Rev. D* **99** (2019) 103513.

[18] E. Babichev, S. Ramazanov and A. Vikman, *JCAP* **1811** (2018) 023.

[19] I. Zlatev, L. M. Wang and P. J. Steinhardt, *Phys. Rev. Lett.* **82** (1999) 896.

[20] R. R. Caldwell, *Phys. Lett. B* **545** (2002) 23.

[21] T. Chiba, T. Okabe and M. Yamaguchi, *Phys. Rev. D* **62** (2000) 023511.

[22] M. C. Bento, O. Bertolami and A. A. Sen, *Phys. Rev. D* **66** (2002) 043507.

[23] S. Tsujikawa, *Class. Quant. Grav.* **30** (2013) 214003.

[24] W. Hu, R. Barkana and A. Gruzinov, *Phys. Rev. Lett.* **85** (2000) 1158.

[25] D. Benisty and E. I. Guendelman, *Phys. Rev. D* **98** (2018) 023506.

[26] D. Benisty, E. Guendelman and Z. Haba, *Phys. Rev. D* **99** (2019) 123521.

[27] F. K. Anagnostopoulos, D. Benisty, S. Basilakos and E. I. Guendelman, *JCAP* **1906** (2019) 003.

[28] D. Benisty and E. I. Guendelman, *Eur. Phys. J. C* **77** (2017) 396.

[29] J. M. M. Senovilla and D. Garfinkle, *Class. Quant. Grav.* **32** (2015) 124008.

[30] A. De Felice and S. Tsujikawa, *Living Rev. Rel.* **13** (2010) 3.

[31] S. Capozziello and M. De Laurentis, *Phys. Rept.* **509** (2011) 167.

[32] S. Nojiri, S. D. Odintsov and V. K. Oikonomou, *Phys. Rept.* **692** (2017) 1.

[33] L. Heisenberg, *Phys. Rept.* **796** (2019) 1.

[34] P. Bull, *et al.*, *Phys. Dark Univ.* **12** (2016) 56.

[35] M. Banados and P. G. Ferreira, *Phys. Rev. Lett.* **105** (2010) 011101.

[36] Y. X. Liu, K. Yang, H. Guo and Y. Zhong, *Phys. Rev. D* **85** (2012) 124053.

[37] T. Harko, F. S. N. Lobo, M. K. Mak and S. V. Sushkov, *Phys. Rev. D* **88** (2013) 044032.

[38] S. W. Wei, K. Yang and Y. X. Liu, *Eur. Phys. J. C* **75** (2015) 253 [erratum: *Eur. Phys. J. C* **75** (2015) 331].

[39] R. Shaikh, *Phys. Rev. D* **92** (2015) 024015.

[40] P. P. Avelino, *Phys. Rev. D* **93** (2016) 044067.

[41] I. Prasetyo, I. Husin, A. I. Qauli, H. S. Ramadhan and A. Sulaksono, *JCAP* **01** (2018) 027.

[42] C. Y. Chen, M. Bouhmadi-López and P. Chen, *Eur. Phys. J. C* **78** (2018) 59.

[43] R. Shaikh, *Phys. Rev. D* **98** (2018) 064033.

[44] S. Jana, R. Shaikh and S. Sarkar, *Phys. Rev. D* **98** (2018) 124039.

[45] C. G. Böhmer and F. Fiorini, *Class. Quant. Grav.* **36** (2019) 12LT01.

[46] P. P. Avelino and R. Z. Ferreira, *Phys. Rev. D* **86** (2012) 041501.

[47] J. Beltrán Jiménez and A. Delhom, *Eur. Phys. J. C* **79** (2019) 656.

[48] J. Beltrán Jiménez, L. Heisenberg, G. J. Olmo and D. Rubiera-García, *Phys. Rept.* **727** (2018) 1.

[49] V. I. Afonso, G. J. Olmo and D. Rubiera-García, *Phys. Rev. D* **97** (2018) 021503.

[50] S. Jana, G. K. Chakravarty and S. Mohanty, *Phys. Rev. D* **97** (2018) 084011.

[51] V. I. Afonso, G. J. Olmo and D. Rubiera-García, *JCAP* **1708** (2017) 031.

[52] L. M. Wang, V. F. Mukhanov and P. J. Steinhardt, *Phys. Lett. B* **414** (1997) 18.

[53] R. Jimenez and A. Loeb, *Astrophys. J.* **573** (2002) 37.

[54] M. Moresco, L. Verde, L. Pozzetti, R. Jimenez and A. Cimatti, *JCAP* **07** (2012) 053.

[55] M. Moresco, *et al.*, *JCAP* **08** (2012) 006.

[56] M. Moresco, *Mon. Not. Roy. Astron. Soc.* **450** (2015) L16.

[57] M. Moresco, *et al.*, *JCAP* **05** (2016) 014.

[58] D. M. Scolnic, *et al.*, *Astrophys. J.* **859** (2018) 101.

[59] F. K. Anagnostopoulos, S. Basilakos and E. N. Saridakis, *Eur. Phys. J. C* **80** (2020) 826.

[60] C. Roberts, K. Horne, A. O. Hodson and A. D. Leggat, [[arXiv:1711.10369](https://arxiv.org/abs/1711.10369) [astro-ph.CO]].

[61] M. Demianski, E. Piedipalumbo, D. Sawant and L. Amati, *Astron. Astrophys.* **598** (2017) A112.

[62] N. B. Hogg, M. Martinelli and S. Nesseris, *JCAP* **12** (2020) 019.

[63] M. Martinelli, *et al.* [EUCLID], *Astron. Astrophys.* **644** (2020) A80.

[64] D. Benisty and D. Staicova, *Astron. Astrophys.* **647** (2021) A38.

[65] W. J. Percival, *et al.* [SDSS], *Mon. Not. Roy. Astron. Soc.* **401** (2010) 2148.

[66] F. Beutler, *et al.*, *Mon. Not. Roy. Astron. Soc.* **416** (2011) 3017.

[67] N. G. Busca, *et al.*, *Astron. Astrophys.* **552** (2013) A96.

[68] L. Anderson, *et al.*, *Mon. Not. Roy. Astron. Soc.* **427** (2013) 3435.

[69] H. J. Seo, *et al.*, *Astrophys. J.* **761** (2012) 13.

[70] A. J. Ross, *et al.*, *Mon. Not. Roy. Astron. Soc.* **449** (2015) 835.

[71] R. Tojeiro, *et al.*, *Mon. Not. Roy. Astron. Soc.* **440** (2014) 2222.

[72] J. E. Bautista, *et al.*, *Astrophys. J.* **863** (2018) 110.

[73] E. de Carvalho, A. Bernui, G. C. Carvalho, C. P. Novaes and H. S. Xavier, *JCAP* **04** (2018) 064.

[74] M. Ata, *et al.*, *Mon. Not. Roy. Astron. Soc.* **473** (2018) 4773.

[75] T. M. C. Abbott, *et al.* [DES], *Mon. Not. Roy. Astron. Soc.* **483** (2019) 4866.

[76] Z. Molavi and A. Khodam-Mohammadi, *Eur. Phys. J. Plus* **134** (2019) 254.

[77] L. Chen, Q. G. Huang and K. Wang, *JCAP* **02** (2019) 028.

[78] D. Foreman-Mackey, D. W. Hogg, D. Lang and J. Goodman, *Publ. Astron. Soc. Pac.* **125** (2013) 306.

[79] W. J. Handley, M. P. Hobson and A. N. Lasenby, *Mon. Not. Roy. Astron. Soc.* **450** (2015) L61.

[80] A. Lewis, [[arXiv:1910.13970](https://arxiv.org/abs/1910.13970) [astro-ph.IM]].

[81] A. G. Riess, *et al.*, *Astrophys. J. Lett.* **908** (2021) L6.

[82] J. Beltrán Jiménez, L. Heisenberg, G. J. Olmo and D. Rubiera-García, *JCAP* **1710** (2017) 029; Erratum: [*JCAP* **1808** (2018) E01].

[83] C. Escamilla-Rivera, M. Banados and P. G. Ferreira, *Phys. Rev. D* **85** (2012) 087302.